AAS 18-370

AN ECLIPTIC PERSPECTIVE FOR ANALYTICAL SATELLITE THEORIES

Ioannis Gkolias[*], Martin Lara[†], and Camilla Colombo[‡]

Traditionally, the forces in analytical theories for Earth satellite orbits are expressed in a coordinate frame which involves the equatorial plane. However, for distant satellites, the Moon and Sun attractions are equally important, and those forces are expressed more conveniently in a frame associated to the ecliptic plane, given that their ephemerides are conveniently represented in this plane. In this work, we develop an analytical satellite theory in which all the forces are expressed with respect to the ecliptic plane. The main advantage of the method is that, after the averaging process, all time-dependent terms disappear from the formulation yielding a model suitable for preliminary orbit design.

INTRODUCTION

Historically, all efforts to analytically study the orbital motion about the Earth have a common starting point, the Main Problem of the artificial satellite theory.[1] And this happens for a good reason, since the perturbations due to the Earth's zonal harmonics are dominant for close Earth satellites. Those perturbations are naturally expressed in an Earth centered coordinate system that uses the equatorial as a reference plane. Therefore, when third-body perturbations due to the Moon and the Sun are also taken into account, they are expressed with respect to that plane.[2] However, the inclination and the node of the Moon, that are needed to estimate its disturbing effect, are expressed as non-linear functions of time with respect to the equator.[3] On the other hand, the lunar inclination is almost constant with respect to the ecliptic and Moon's node is a linear function of time on the ecliptic. For this reason, it is a common approach in the analytical approach to apply a series of geometrical transformations, such that, the ecliptic Moon's elements finally appear in the expression of the disturbing potential.[4,5]

In this work, we will take a slightly different approach compared to the traditional one in the literature. Namely, we will assume a reference frame which has the ecliptic as the fundamental plane. The two approaches are equivalent from a physical point of view,

[*]PhD, Research Fellow, Department of Aerospace Science and Technology, Politecnico di Milano, Via La Masa 34, 20156, Milano, Italy. email:ioannis.gkolias@polimi.it

[†]PhD, Associate Researcher, GRUCACI, University of La Rioja, C/ Madre de Dios, 53, ES-26006 Logroño, Spain. Tel. (+34) 941299440, email: mlara0@gmail.com

[‡]PhD, Associate Professor, Department of Aerospace Science and Technology, Politecnico di Milano, Via La Masa 34, 20156, Milano, Italy. email:camilla.colombo@polimi.it

but in a perturbation approach there exist relevant differences that we will try to exploit. In particular, in the ecliptic frame formulation, the analytical expansions for the lunisolar perturbations simplify. On the contrary, the perturbations due to the zonal harmonics of Earth's gravitational field now become more involved than in the equatorial plane formulation, because a further rotation of the reference frame is needed. The effect of this additional rotation is to increase the number of terms of this perturbation which have the right ascension of the ascending node (RAAN) of the satellite as an additional argument of the trigonometric functions. However, the balance is beneficial in some cases of interest.

The total disturbing potential, expressed in the ecliptic reference frame, will be averaged over the fast angles. First, the dependence on the mean anomaly of the satellite will be removed, via a standard closed form averaging procedure.[6,7] Then the effect due to the mean anomaly of the Moon is as well averaged, also in closed form. The double averaged Hamiltonian[8,9] still depends on the argument of the perigee and RAAN of the satellite, and of the time —the latter explicitly appearing in the ecliptic longitude of the Sun, and the RAAN of the Moon orbit on the ecliptic. However, the time dependence of the long-term resulting Hamiltonian can be avoided by a further averaging. Indeed, in view of the ecliptic plane formulation both time-dependent angles are defined in the same plane as the satellite's RAAN. Therefore, when a third averaging is done over the ecliptic node of the satellite, both the time dependencies and the RAAN of the satellite disappear from the triple averaged model. This corresponds to an elimination of the node procedure, frequently introduced in analytical investigations.[10,11]

The resulting approximate model is autonomous and one degree of freedom, thus it can be used to study the long term behaviour of distant Earth satellites. One immediate application of such a model is the preliminary design of frozen and disposal orbits.[12,13] Those appear as particular solutions of the reduced model.

MODEL FORMULATION

The orbit of a massless Earth's satellite can be modelled as a perturbed Keplerian motion,

$$\mathcal{H} = H_{\text{kep}} + H_{\text{zonal}} + H_{\text{third-body}}. \tag{1}$$

In the above equation, the term H_{kep} is simply the Keplerian one

$$H_{\text{kep}} = -\frac{\mu}{2a},$$

where μ is Earth's gravitational parameter and a is the satellite's semi-major axis. The non-centralities of Earth's gravitational field and are modelled from the potential[6]

$$H_{\text{zonal}} = -\frac{\mu}{r}\sum_{j\geq 2}\left(\frac{R_\oplus}{r}\right)^j C_{j,0}P_{j,0}(\sin\phi), \tag{2}$$

where $R_\oplus = 6378.1\ km$ is the mean equatorial radius of the Earth, ϕ the geometric latitude of the satellite, $C_{j,0}$ the zonal harmonic coefficients and $P_{j,0}$ are the zeroth order associated

Legendre polynomials of degree j. Finally, the third body perturbations are modelled as a series expansion in the parallactic ratio $(r/r')^6$

$$H_{\text{third-body}} = -\frac{\mu'}{r'} \sum_{j \geq 2} \left(\frac{r}{r'}\right)^j P_j(cos\psi), \tag{3}$$

where μ' is the third body's gravitational parameters, r and r' the distance of the satellite and the third body from center of the Earth respectively, P_j are the Legendre polynomials and ψ is the angle between the position of the satellite and the third body as viewed from the Earth.

In order to develop our analytical theory, we will need to express the positions of the involved bodies with respect to our coordinate system. Ideally we would like to have the Cartesian coordinates expressed as functions of the orbital elements. This is easy to do by employing a series of geometrical rotations either along the x-axis R_1 or the z-axis R_3 of our system.

The position of the satellite, in Cartesian coordinates (x, y, z), can be expressed in the Earth ecliptic plane in terms of its orbital elements as

$$\begin{pmatrix} x \\ y \\ z \end{pmatrix} = R_3(-\Omega)R_1(-i)R_3(-\theta) \begin{pmatrix} r \\ 0 \\ 0 \end{pmatrix} \tag{4}$$

where r is the distance of the satellite from the Earth, θ the argument of the latitude, i the inclination and Ω the RAAN of the satellite. We should mention here that all the angles are measured with respect to the ecliptic frame. The position of the Sun, in Cartesian coordinates $(x_\odot, y_\odot, z_\odot)$, is given simply from the relation

$$\begin{pmatrix} x_\odot \\ y_\odot \\ z_\odot \end{pmatrix} = R_3(-\theta_\odot) \begin{pmatrix} r_\odot \\ 0 \\ 0 \end{pmatrix} \tag{5}$$

where $r_\odot$ is the Sun-Earth distance and $\theta_\odot$ is argument of Sun's latitude. Similarly for the Moon, we have that its position $(x_{\leftmoon}, y_{\leftmoon}, z_{\leftmoon})$ in the ecliptic frame is given from

$$\begin{pmatrix} x_{\leftmoon} \\ y_{\leftmoon} \\ z_{\leftmoon} \end{pmatrix} = R_3(-\Omega_{\leftmoon})R_1(-i_{\leftmoon})R_3(-\theta_{\leftmoon}) \begin{pmatrix} r_{\leftmoon} \\ 0 \\ 0 \end{pmatrix} \tag{6}$$

where $r_\odot$ is the Moon-Earth distance, $\theta_{\leftmoon}$ is the argument of Moon's latitude, $\Omega_{\leftmoon}$ is the longitude of the ascending node of the Moon's orbit on the ecliptic plane and is a linear function of time, and $i_{\leftmoon}$ is the inclination of the Moon's orbit over the ecliptic, which can be considered constant equal to approximately 5.1°.

Finally, the equatorial (ξ, η, ζ) fixed frame coordinates of the satellite are expressed with respect to the ecliptic ones as

$$\begin{pmatrix} \xi \\ \eta \\ \zeta \end{pmatrix} = R_1(-\epsilon) \begin{pmatrix} x \\ y \\ z \end{pmatrix}, \tag{7}$$

where ϵ is the obliquity of the ecliptic and is considered constant $\epsilon = 23.4°$.

In order to proceed with the averaging process we assume the quadrupolar expansion with respect to the Earth's gravitational expansion and third body perturbations. Under this assumption the zonal part of the Hamiltonian reads

$$H_{J_2} = \frac{\mu}{r}\left(\frac{R_\oplus}{r}\right)^2 J_2 P_2(\sin\phi) \tag{8}$$

where $J_2 = -C_{2,0} = 1082.63 \cdot 10^{-6}$ and the sinus of the latitude of the satellite $\sin\psi$ is given from the relation

$$\sin(\phi) = \frac{\zeta}{r} = \frac{z\cos(\epsilon) + y\sin(\epsilon)}{r}. \tag{9}$$

We proceed with an averaging, in closed form, over the satellite's mean anomaly M to get

$$\bar{H}_{J_2} = \bar{H}_{J_2}(a, e, i, \Omega, -, -; \mu, J_2, R_\oplus, \epsilon) \tag{10}$$

or in explicit form

$$\bar{H}_{J_2} = \frac{R_\oplus^2 J_2 \mu}{a^3\eta^3}\left(\frac{3}{2}c_\epsilon c_i s_i s_\epsilon \cos(\Omega) - \frac{3}{8}s_i^2 s_\epsilon^2 \cos(2\Omega) + \frac{1}{8}\left(2 - 3s_i^2\right)\left(3s_\epsilon^2 - 2\right)\right), \tag{11}$$

where $s_i, c_i, s_\epsilon, c_\epsilon$ are the cosine and sine functions of the satellite's inclination i and the obliquity of the ecliptic ϵ, and $\eta = \sqrt{1-e^2}$.

Notice here, that unlike in the equatorial first-order averaged J_2 potential, the ecliptic one in Equation (11) is still depended on the ecliptic node of the satellite Ω. However, we will see how do deal with those terms in the following. In fact, the more convenient form of the third-body averaged potential will compensate for this fact.

The Sun's perturbing potential is

$$H_\odot = -\frac{n_\odot a_\odot^3}{r_\odot}\left(\frac{r}{r_\odot}\right)^2 P_2(cos\psi_\odot) \tag{12}$$

where $n_\odot$ is the mean motion the Earth orbiting around the Sun and $a_\odot$ the semi-major axis equal approximately to one Astronomical Unit ($149598023\ km$) . The cosine of the angle ψ between the position vectors of the satellite and the Sun in the geocentric ecliptic frame is given from

$$\cos(\psi_\odot) = \frac{xx_\odot + yy_\odot + zz_\odot}{rr_\odot}, \tag{13}$$

where the coordinates of the satellite and the Sun are given for Equation (4) and Equation (5) respectively.

As for the zonal case, we average in closed form over the satellite's mean anomaly and the single-averaged potential is

$$\bar{H}_{\odot} = \bar{H}_{\odot}(a, e, i, \Omega, \omega, -, \theta_{\odot}; n_{\odot}, a_{\odot}),$$

or in explicit form

$$\begin{aligned}
\bar{H}_{\odot} = &-\frac{15}{32} a^2 e^2 n_{\odot}^2 \left(c_i - 1\right)^2 \cos(2\theta_{\odot} + 2\omega - 2\Omega) \\
&-\frac{15}{32} a^2 e^2 n_{\odot}^2 \left(c_i + 1\right)^2 \cos(2\theta_{\odot} - 2\omega - 2\Omega) \\
&-\frac{1}{16} a^2 \left(3e^2 + 2\right) n_{\odot}^2 \left(3c_i^2 - 1\right) \\
&-\frac{3}{16} a^2 \left(3e^2 + 2\right) n_{\odot}^2 s_i^2 \cos(2\theta_{\odot} - 2\Omega) \\
&-\frac{15}{16} a^2 e^2 n_{\odot}^2 s_i^2 \cos(2\omega),
\end{aligned} \tag{14}$$

where again c_i, s_i are the cosine and sine of the inclination i. Finally, for the Moon's perturbation we have

$$H_{\leftmoon} = -\beta \frac{n_{\leftmoon}\, a_{\leftmoon}^3}{r_{\leftmoon}} \left(\frac{r}{r_{\leftmoon}}\right)^2 P_2(cos\psi_{\leftmoon}) \tag{15}$$

where $n_{\leftmoon}$ is the mean motion the Moon orbiting around the Earth and $a_{\leftmoon} = 384399\ km$ the semi-major of Moon's orbit. The cosine of the angle ψ between the position vectors of the satellite and the Moon in the geocentric ecliptic frame is given from

$$\cos(\psi_{\leftmoon}) = \frac{x x_{\leftmoon} + y y_{\leftmoon} + z z_{\leftmoon}}{r r_{\leftmoon}}, \tag{16}$$

where the coordinates of the satellite and the Moon are given for Equation (4) and Equation (6) respectively. Like we did with the Sun's perturbing potential, we average in closed form over the satellite's mean anomaly to get

$$\bar{H}_{\leftmoon} = \bar{H}_{\leftmoon}(a, e, i, \Omega, \omega, -, \Omega_{\leftmoon}, \theta_{\leftmoon}; \beta, n_{\leftmoon}, a_{\leftmoon}, i_{\leftmoon}). \tag{17}$$

However, for the case of the Moon, we will need to perform a second averaging to further proceed with our analytical investigation. Unlike in the case of the Sun's argument of latitude $\theta_{\odot}$, the one of the Moon $\theta_{\leftmoon}$ enters the equations through a geometrical relation that does not always couple it with that of the ecliptic RAAN Ω of the satellite. Therefore, we proceed to eliminate this frequency, by a second averaging, also in closed form, this time performed over the Moon's mean anomaly. The double averaged perturbing function for the Moon now reads

$$\bar{\bar{H}}_{\leftmoon} = \bar{\bar{H}}_{\leftmoon}(a, e, i, \Omega, \omega, -, \Omega_{\leftmoon}, -; \beta, n_{\leftmoon}, a_{\leftmoon}, i_{\leftmoon}, \eta_{\leftmoon}), \tag{18}$$

or in explicit form

$$\begin{aligned}\bar{\bar{H}}_{\leftmoon} = \frac{a^2\beta n_{\leftmoon}^2}{64\eta_{\leftmoon}^3}\Big[&-15e^2\left(c_i-1\right)^2 s_{i_{\leftmoon}}^2\ \cos(2(\Omega_{\leftmoon}+\omega-\Omega))\\ &-15e^2\left(c_i+1\right)^2 s_{i_{\leftmoon}}^2\ \cos(2(\Omega_{\leftmoon}-\omega-\Omega))\\ &+60e^2\left(c_i-1\right)c_{i_{\leftmoon}}\ s_i s_{i_{\leftmoon}}\ \cos(\Omega_{\leftmoon}+2\omega-\Omega)\\ &+60e^2\left(c_i+1\right)c_{i_{\leftmoon}}\ s_i s_{i_{\leftmoon}}\ \cos(\Omega_{\leftmoon}-2\omega-\Omega)\\ &-24\left(3e^2+2\right)c_i c_{i_{\leftmoon}}\ s_i s_{i_{\leftmoon}}\ \cos(\Omega_{\leftmoon}-\Omega)\\ &-30e^2\left(3c_{i_{\leftmoon}}^2-1\right)s_i^2\cos(2\omega)\\ &-2\left(3e^2+2\right)\left(3c_i^2-1\right)\left(3c_{i_{\leftmoon}}^2-1\right)\\ &-6\left(3e^2+2\right)s_i^2 s_{i_{\leftmoon}}^2\ \cos(2(\Omega_{\leftmoon}-\Omega))\Big],\end{aligned} \tag{19}$$

where $c_i, s_i, c_{i_{\leftmoon}}, s_{i_{\leftmoon}}$ are the cosine and sine functions of the satellite's and Moon's inclination respectively and $\eta_{\leftmoon} = \sqrt{1-e_{\leftmoon}^2}$.

Putting all the averaged contributions together we get

$$\bar{\bar{H}} = \bar{H} + \bar{H}_{\odot} + \bar{\bar{H}}_{\leftmoon},$$

which is still a non-autonomous two degrees of freedom system,

$$\bar{\bar{H}} = \bar{\bar{H}}(a, e, i, \Omega, \omega, -, \Omega_{\leftmoon}(t), \theta_{\odot}(t); \mu, J_2, R_{\oplus}, \epsilon, n_{\odot}, a_{\odot}, n_{\leftmoon}, a_{\leftmoon}, i_{\leftmoon}, \eta_{\leftmoon}).$$

Since the mean anomaly of the satellite has been averaged throughout the equations the semi-major axis is constant and therefore the motion takes place in 4-dimensional phase space (e, i, ω, Ω) and we still have the time-periodic dependencies from the ecliptic node of the Moon $\Omega_{\leftmoon}(t)$ and the argument of latitude of the sun $\theta_{\odot}(t)$ that add two additional extra frequencies to the system. This system is very similar to the one obtained in the equatorial single-averaged problem. However, in the ecliptic representation, there is an important a feature that we will exploit. By a careful inspection of Equations (11),(14) and (19) we notice that the time-dependent arguments appear always coupled with the satellite's *ecliptic node* Ω.

Therefore, we can proceed with a further *elimination of the ecliptic node*. This is accomplished by working in a suitable rotating frame and is a valid operation when the perturbations are *of the same order*, i.e. for distant Earth's satellites. After this procedure the averaged perturbations read

$$\bar{\bar{H}}_{J_2} = \frac{J_2 R_{\oplus}^2 \mu (3\cos^2 i - 1)(3\sin^2\epsilon - 2)}{8a^3\eta^3}$$

$$\bar{\bar{H}}_{\odot} = a^2 n_{\odot}^2 \left(-\frac{15}{16} e^2 \cos 2\omega \sin^2 i + \frac{1}{16}(2+3e^2)(3\sin^2 i - 2) \right)$$ [8]

$$\bar{\bar{H}}_{\leftmoon} = -\frac{a^2 n_{\leftmoon}^2 \, \beta (3\cos^2 i_{\leftmoon} - 1)((2+3e^2)(3\cos^2 i - 1) + 15e^2 \sin^2 i \cos 2\omega)}{32\eta_{\leftmoon}^3}$$

Finally, adding all the perturbing effects we obtain the triple averaged approximation, which results in a one degree of freedom Lidov-Kozai[10,11] type Hamiltonian

$$\bar{\bar{H}} = \frac{A}{\eta^3}(2 - 3\sin^2 i) + B((2+3e^2)(2-3\sin^2 i) + 15e^2 \sin^2 i \cos 2\omega)$$

where

$$A = -\frac{J_2 R_{\oplus}^2 \mu}{8a^3}(2 - 3\sin^2 \epsilon)$$

and

$$B = -\frac{1}{16}\left(n_{\odot}^2 + \frac{n_{\leftmoon}^2}{\eta_{\leftmoon}} \beta \frac{3\cos^2 i_{\leftmoon} - 1}{2} \right) a^2$$

The system no longer depends on the mean anomaly M and the ecliptic RAAN of the satellite Ω, therefore there are two integral of the motion: the semi-major axis a is constant and also the Lidov-Kozai's integral[10,11]

$$\sqrt{1-e^2}\cos i = \text{constant} \tag{20}$$

is also constant. The two quantities constitute the fundamental dynamical parameters of our system. The triple averaged system can be studied completely analytical and provides an integrable approximation of the full problem, suitable to understand the underlying mechanisms and enhance the preliminary mission design process.

PHASE SPACE STUDY

We proceed with the phase-space study of the triple averaged model derived in this work, in order to understand the underlying dynamics for different values of the dynamical parameters. The solutions of the systems are represented as level curves for the one degree of freedom, triple averaged model in the (e, ω) plane. For convenience, we prefer to study the evolution in non-singular elements

$$k = e\cos\omega, \; h = e\sin\omega$$

and the equations of motion are

$$\frac{dk}{dt} = -\frac{\sqrt{1-h^2-k^2}}{na^2}\frac{dV(k,h)}{dh}$$
$$\frac{dh}{dt} = \frac{\sqrt{1-h^2-k^2}}{na^2}\frac{dV(k,h)}{dk}$$

where is $V = \bar{\bar{\bar{H}}}(k(e,\omega), h(e,\omega))$ the triple averaged disturbing function expressed as a function of the non-singular elements. The equilibrium points are solutions of the system

$$dk/dt = dh/dt = 0,$$

and their stability is determined from the eigenvalues of the linearised system of the right-hand side of the equations of motion. As we have discussed, there are two conserved quantities in the system and their initial values are defined from the value of the semi-major axis and the initial value of the Lidov-Kozai integral $\sqrt{1-e^2}\cos i$. For the second we choose its value as the inclination of the circular $e = 0$ orbits. More specifically, in order to select a specific value of the second integral we set in Equation (20) the eccentricity equal to zero and we substitute any instance of the $\cos i$ in the triple averaged model through the relationship

$$\sqrt{1-e^2}\cos(i) = \cos(i_{\text{circ}}) \Rightarrow \cos i = \frac{\cos(i_{\text{circ}})}{\sqrt{1-e^2}}.$$

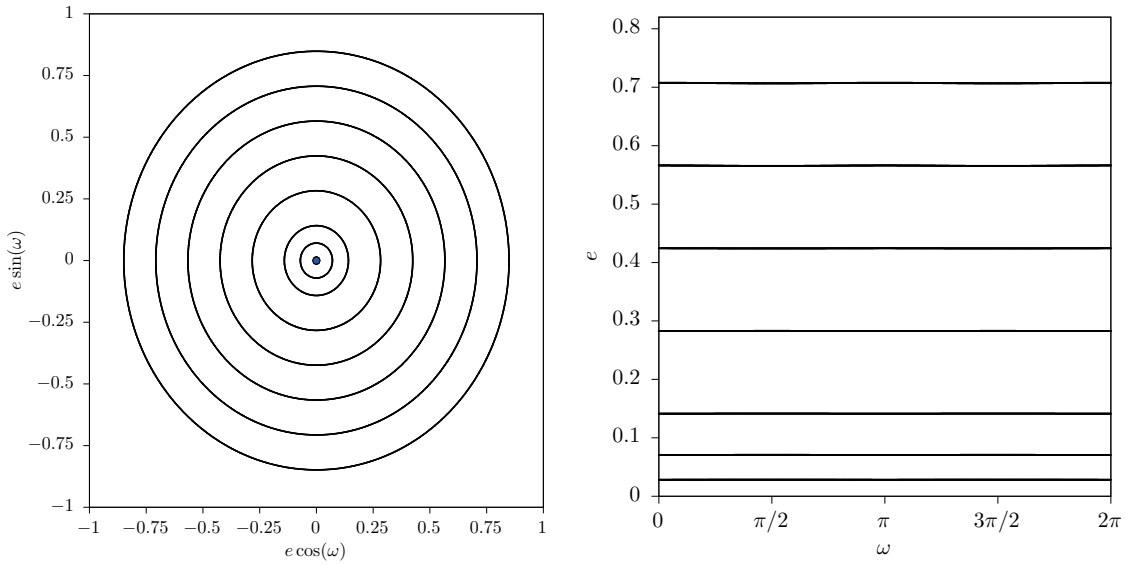

Figure 1. The phase-space at $a = 20000\ km$ and $i_{\text{circ}} = 20°$, typical for low inclinations at all altitudes. The blue dot corresponds to the equilibrium solution for circular orbits.

Varying the values of the dynamical parameters, four different topologies are encountered. Those are depicted in Figures 1-4. Starting from low i_{circ} the picture of the in-plane dynamics is quite calm as seen in Figure 1. The circular orbits are the only equilibrium of the system, and the value of the averaged eccentricity is almost constant along any other initial conditions. This picture holds for all altitudes at low inclinations, up to a value of about $40° - 63°$ depending on the altitude.

Moving to medium inclinations, from a value of $40°$ inclination and above the phase space changes dramatically. In Figure 2 we present the phase space topology for this case. First, two more stable equilibrium solutions appear, whereas the equilibrium corresponding

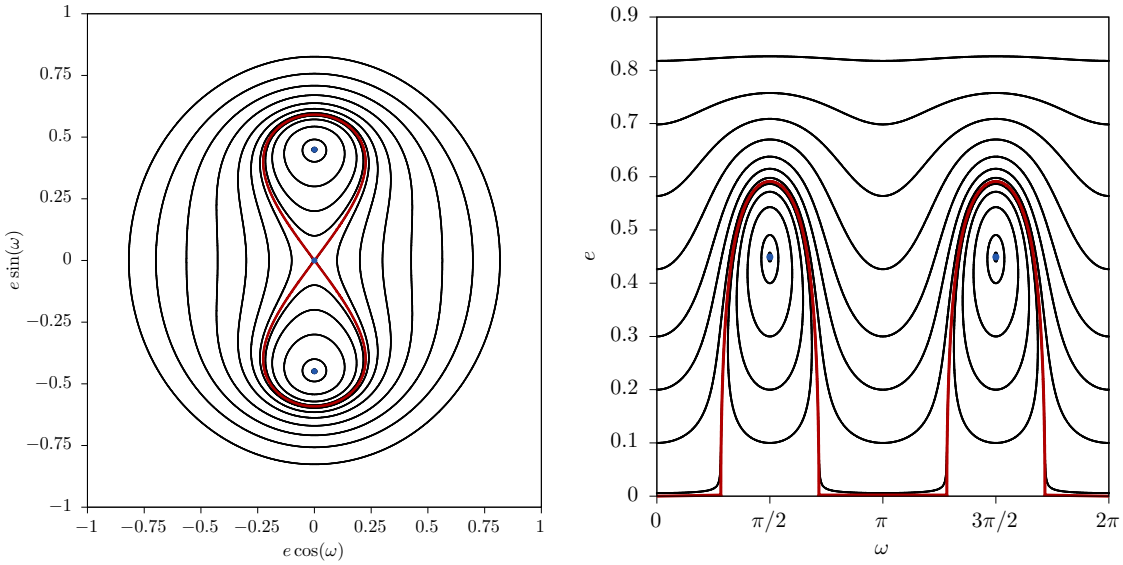

Figure 2. The phase-space at $a = 30000\ km$ and $i_{\text{circ}} = 60°$, typical for moderate inclinations at all altitudes. The blue dots correspond to the three equilibrium solutions and the red line represents the separatrix of the unstable point.

to circular orbits has become unstable. This phenomena is knows as a *pitchfork bifurcation*. The separatrix emanating from zero eccentricity, allow almost circular orbits to exhibit large eccentricity variations within a period of their perigee oscillation. On the other hand, there appear now, two frozen eccentric orbits for $\omega = \pi/2$ and $3\pi/2$. The red line in Figure 2 represents the separatrix of unstable equilibrium that appears for the circular orbits. While in Figure 1 all solution have an argument of perigee that rotates, in this case we have also the option of librational motion within the lobes of the eight-shape figure of the separatrix. Therefore, the separatrix is actually dividing the phase space to librational (inside) and rotational (outside) behaviour of the ecliptic argument of perigee ω.

At medium altitudes, between 20000 and $35000\ km$, the picture changes one more time when we further increase the inclinations towards even higher values. In Figure 3 we see that another pitchfork bifurcations occurs, rendering the circular orbits stable again. The two eccentric frozen orbit solutions still exist at $\omega = \pi/2$ and $3\pi/2$, but there are now also two unstable eccentric frozen orbits for $\omega = 0$ and π respectively.

Finally, the situation for high inclinations at higher altitude values is presented in Figure 4. This situation can be reached either by increasing the value of the altitude of an initially inclined orbit or increasing the inclination at an already high altitude. The transition in the first case is done through another pitchfork bifurcation for the circular orbits, which become unstable again while a pair of eccentric frozen orbits at $\omega = 0$ and π appear. In the later case, one can reach this particular phase space through two tangent (saddle-node) bifurcations. In this case two pairs of equilibria, one stable and unstable, appear from the rectilinear orbits, i.e. orbits with $e = 1$ which are represented by the unit circle in the (h, k)-plane.

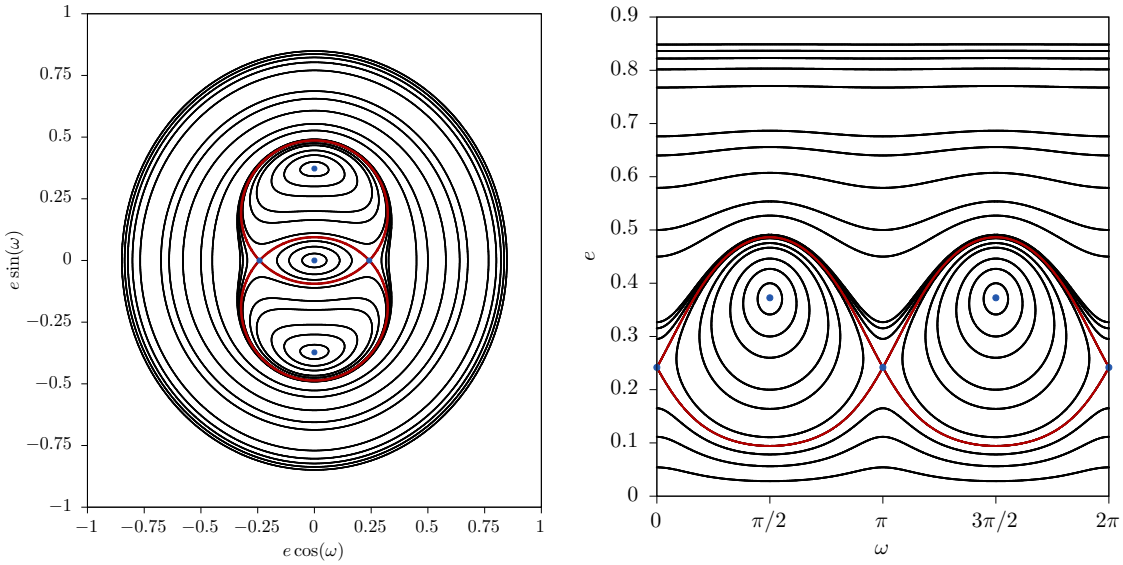

Figure 3. The phase-space at $a = 20000\ km$, $i_{\text{circ}} = 65°$, typical for high inclinations at medium altitudes . The blue dots correspond to the five equilibrium solutions and the red lines represent the separatrices of the unstable points, which form a heteroclinic connection in the phase space.

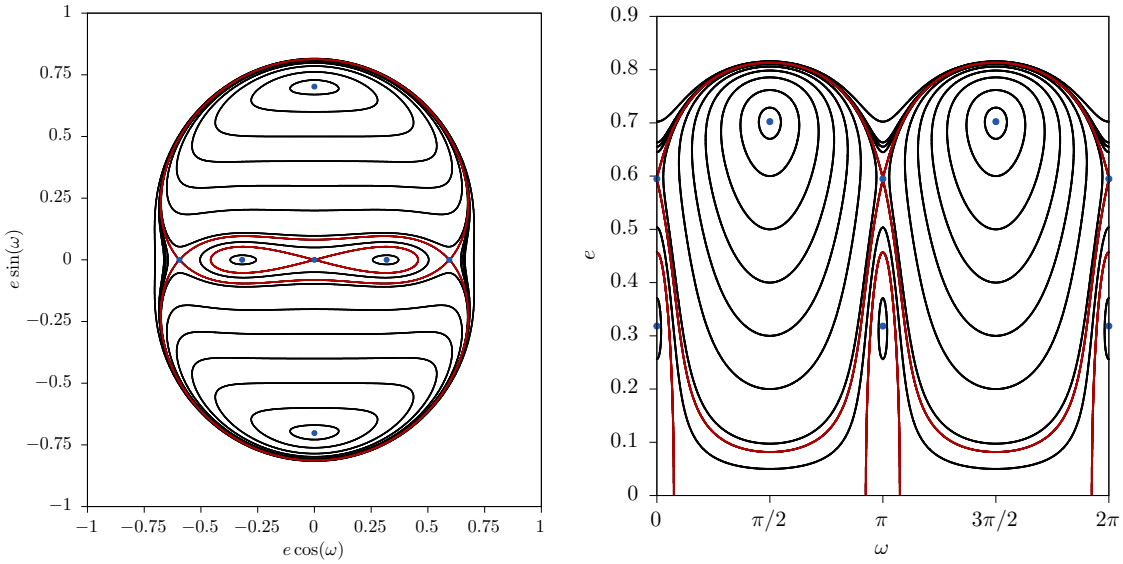

Figure 4. The phase-space at $a = 40000\ km$ and $i_{\text{circ}} = 70°$, typical for high inclinations at high altitudes . The blue dots correspond to the seven equilibrium solutions and the red lines represent the separatrices of the unstable points. The inner separatrix stems from the unstable circular orbits while the outer one forms a heteroclinic connection between the remaining unstable equilibria.

All the phase space transitions are summarised in Figure 5, where we present the bifurcation diagram for the triple averaged model in the dynamical parameter space (a, i_{circ}). What we are actually observing is the interplay between the J_2 and the third-body perturbations. For inclinations smaller that 40 degrees or higher than 140, all orbits are stable with low

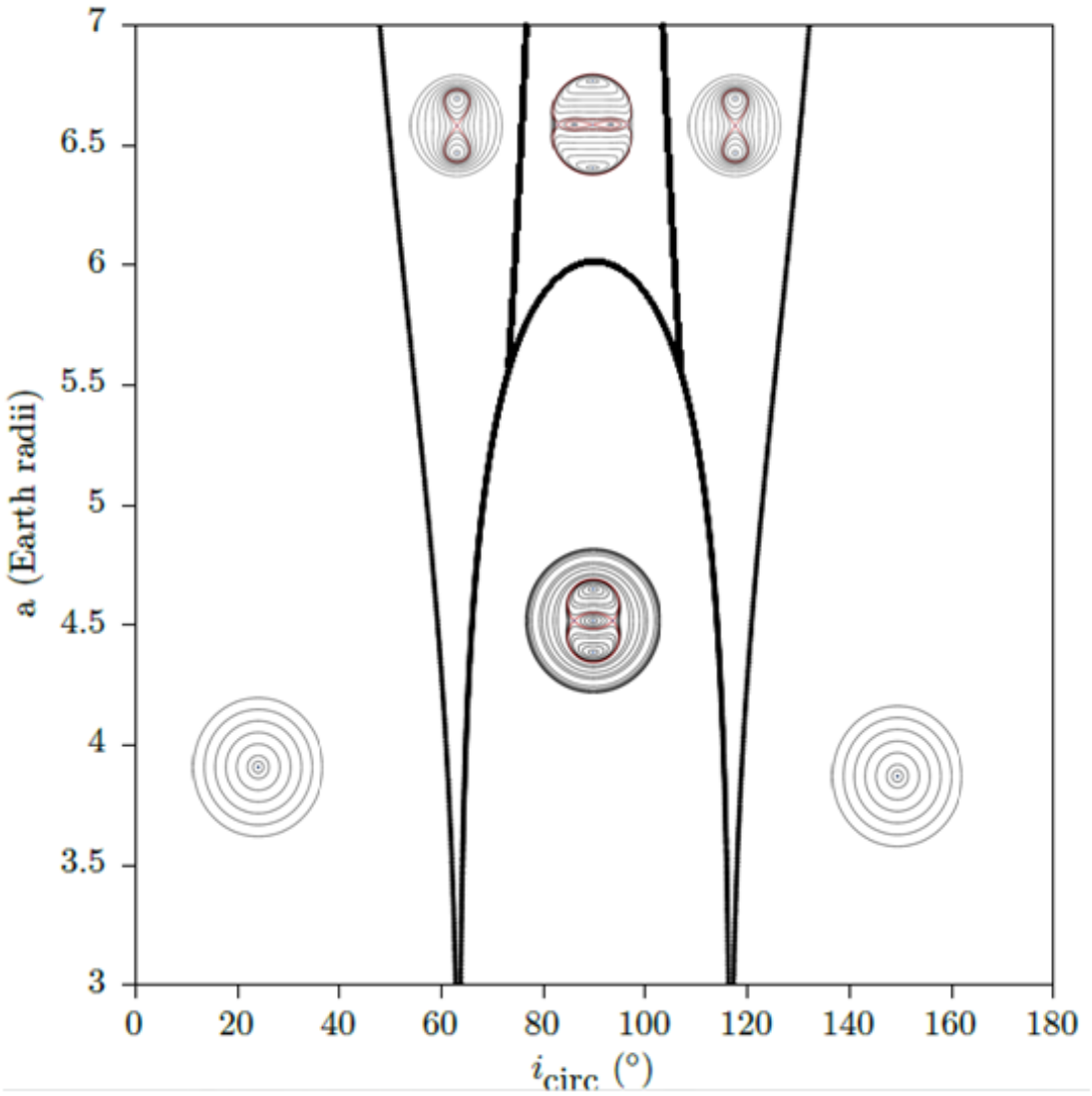

Figure 5. The bifurcation diagram for the different types of motion in the dynamical parameter space (a, i_{circ}).

eccentricity variations. For inclinations between $40 - 140$ degrees, there is a competition between the Lidov-Kozai mechanism induced by the Sun and the Moon and the contribution of J_2. More specifically, it is know that the planet's oblateness J_2 can suppress[14] the effect and stabilise all initially circular orbits. We find this to happen for Earth orbiters up to semi-major axis values of 6 Earth radii. An exception appears in the case of orbits of about 63° inclination which corresponds to the critical inclination resonance. For semi-major axis higher than 6 Earth radii, the situation changes, as the third body effects dominate, and initially circular orbits are unstable for a wide range of inclinations. This transition, creates a natural transition from stability to instability for inclined orbits, as moving further away from the Earth. However, within the unstable domain, there do exist a variety of stable frozen orbit solutions which could be exploited for interesting mission design purposes.

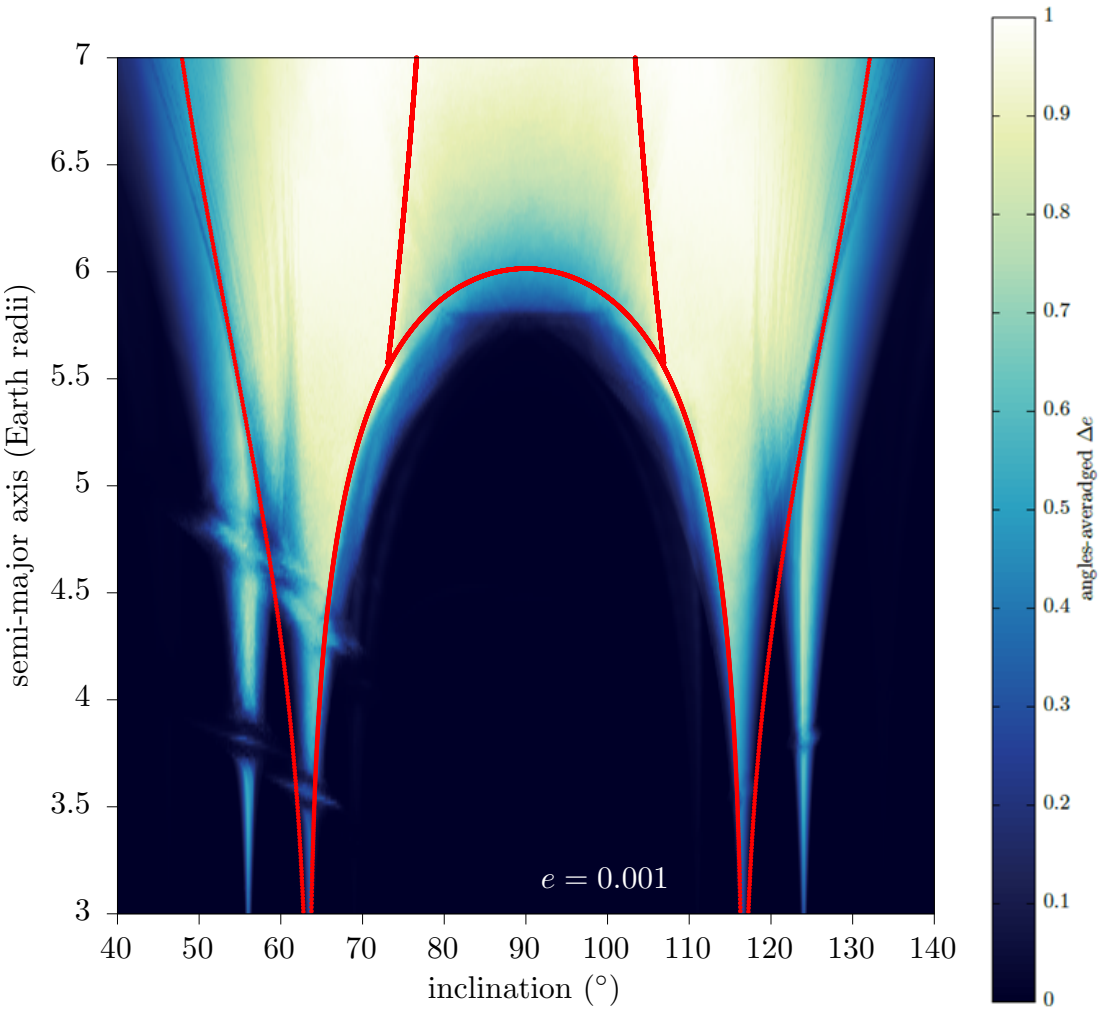

Figure 6. Comparison between the analytical bifurcation limit and numerically obtained stability map. The red-line corresponds to the analytical bifurcation limit computed via the triple-averaged model. The background colormap gives the normalised eccentricity diameter Δe averaged over a set of 50 randomly set of angles for each point in the action-like space $(a - e - i)$.

As a final verification of our model, we proceed with a comparison of our analytical results about the stability of circular orbits of Earth's orbiters with numerical propagation of the double-averaged dynamics.[15] In Figure 6 we superpose the analytical bifurcation curve, obtained with the triple-averaged model to a numerically obtained dynamical map for almost circular orbits. The numerically averaged map is obtained by propagating for each point in the action-like space (a, e, i) a set of 50 randomly selected angular configurations $(\Omega, \omega, \Omega_{\mathbb{C}})$. For each of the orbits we compute a *normalised eccentricity diameter* defined as:[15]

$$\Delta e = \frac{|e_0 - e_{\text{max}}|}{|e_0 - e_{\text{re-entry}}|} \tag{21}$$

where e_{max} is the maximum value of the eccentricity obtained in the timespan of the numerical propagation (typically about 45 lunar node periods $\approx 450\ y$), e_0 the initial value of

the eccentricity and $e_{\text{re-entry}}$ the value of the eccentricity for which the re-entry condition is met for each semi-major axis.

Since we are interested in the stability of initially circular orbits, the grid of dynamical map in Figure 6 is over semi-major axis a and the initial inclination of the orbit. Then for each point we take the mean value of Δe over the ensemble of the angular configurations. The level of matching between our analytical results and the numerical result is striking. We recall here that in the analytical approximation, circular orbits outside the left-most and right-most arcs, as well as within the central arc are stable. The rest correspond to orbit where the simplified dynamics predicts high eccentricity excursions for circular orbits (see also Figure 5). The simple triple-averaged model captures very well the transition from stability to instability for inclined Earth orbits as the semi-major axis increases.

Of course there are features in the full model, which are not captured in our simplified model. For example the unstable domain around the 57° inclination is known to be related with the term including the $2\omega + \Omega$ of the satellite. This kind of terms are absent from our triple-averaged model and so their dynamics is not included in our study. However, our model captures the main features around the critical inclination resonance and its transition to a Lidov-Kozai instability at higher altitudes.

FROZEN AND DISPOSAL ORBIT DESIGN

The triple averaged Hamiltonian obtained in the previous section, can be used for preliminary design of distant frozen orbits. Namely, we are looking for orbit with constant perigee, which are simply the stationary solutions of the $\bar{\bar{\bar{\mathcal{H}}}}$. There are two different types of frozen solutions: one with $\omega = \pi/2$ or $3\pi/2$ and one $\omega = 0$ and π. Those can be exploited depending on the type of mission.

Another way we could use the insight information provided by the triple averaged model, is to design end-of-life disposal orbits for high Earth satellites. Let us assume a semi-major axis of about 40000 km, then the different phase spaces with respect to i_{circ} are presented in Figure 7. We show the different evolutions of an initial circular $e = 0$ and a moderately eccentric orbit $e = 0.2$ orbit due to the increase in i_{circ}. For $i_{\text{circ}} < 40^\circ$ the circular orbit is stable and orbit with $e = 0.2$ undergoes some small eccentricity variations. However, after an $i_{\text{circ}} \approx 50\,\text{deg}$, both initial orbits exhibit significant variations in the eccentricity. These eccentricity variations keep increasing and allow us to reach even an atmospheric re-entry value* within the first period of the ω oscillation. In the meantime, stable frozen orbits co-exist in these configurations, for particular values of the eccentricity. A mission design concept that exploits the stable equilibria during the operational lifetime, and the unstable equilibria for a re-entry at end-of-life can become a new paradigm for a sustainable exploitation of distant Earth orbits.

*The re-entry altitude in this work is set to $120\ km$ above the Earth's surface

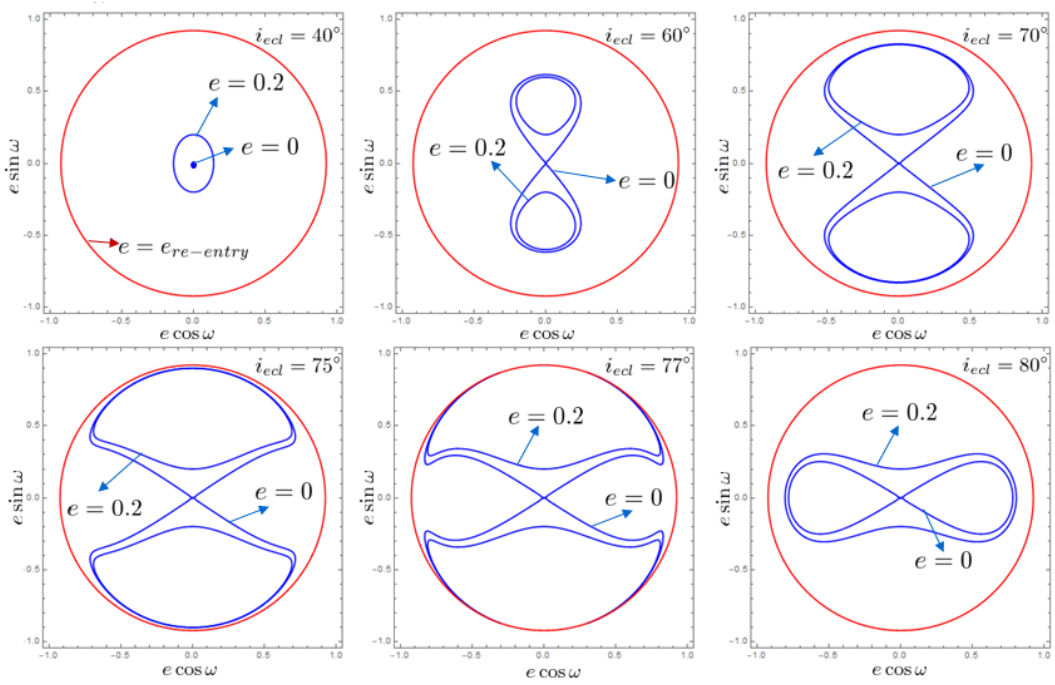

Figure 7. Frozen orbit and disposal design based on the 1 degree of freedom simplified Hamiltonian.

CONCLUSION

In this work, we have averaged the problem of high Earth satellites using an ecliptic representation of a quadrupolar approximation of the force model. The resulting 1 degree of freedom system, resembles a Lidov-Kozai approximation for the case of the Earth and describes the in-plane stability of the orbits. We have studied the reduced phase-space by computing the equilibrium points and their stability and we have calculated the bifurcation diagram for the different types of behaviour. Moreover, this simplified model gives us some analytical insight for the orbital stability in the regions of its validity. This information could be exploited in orbit design of distant Earth satellites.

As further work, we will recover the short-periodic terms of transformations involved in the triple-averaged approximation. This will help us to compare the analytical results with orbits in the full model and allow us to check if they hold the desired properties, i.e. small eccentricity variations for the frozen orbit design case and short lifetimes for the preliminary disposal design case. Moreover, additional perturbation terms can be added in our model to make the approximation more accurate, namely the second order J_2^2 and the forth order Legendre polynomial P_4 for the Moon's attraction.[16,17] Finally, the ultimate goal of this analytical treatment, is to allow us to enhance the current mission design process for distant Earth's satellites.

ACKNOWLEDGMENTS

This project has received funding from the European Research Council (ERC) under the European Union's Horizon 2020 research and innovation programme (grant agreement No 679086 – COMPASS).

REFERENCES

[1] D. Brouwer, "Solution of the problem of artificial satellite theory without drag," *The Astronomical Journal*, Vol. 64, Nov. 1959, p. 378, 10.1086/107958.

[2] W. M. Kaula, "Development of the lunar and solar disturbing functions for a close satellite," *The Astronomical Journal*, Vol. 67, June 1962, p. 300, 10.1086/108729.

[3] G. E. Cook, "Luni-Solar Perturbations of the Orbit of an Earth Satellite," *Geophysical Journal*, Vol. 6, Apr. 1962, pp. 271–291, 10.1111/j.1365-246X.1962.tb00351.x.

[4] G. E. O. Giacaglia, "Lunar Perturbations of Artificial Satellites of the Earth," *Celestial Mechanics*, Vol. 9, Apr. 1974, pp. 239–267, 10.1007/BF01260515.

[5] M. T. Lane, "On analytic modeling of lunar perturbations of artificial satellites of the earth," *Celestial Mechanics and Dynamical Astronomy*, Vol. 46, 1989, pp. 287–305, 10.1007/BF00051484.

[6] M. Lara, J. F. San-Juan, L. M. López, and P. J. Cefola, "On the third-body perturbations of high-altitude orbits," *Celestial Mechanics and Dynamical Astronomy*, Vol. 113, Aug 2012, pp. 435–452, 10.1007/s10569-012-9433-z.

[7] M. Lara, J. F. San-Juan, L. M. López-Ochoa, and P. Cefola, "Long-term evolution of Galileo operational orbits by canonical perturbation theory," *Acta Astronautica*, Vol. 94, No. 2, 2014, pp. 646 – 655, https://doi.org/10.1016/j.actaastro.2013.09.008.

[8] P. E. El'yasberg, "Introduction to the Theory of Flight of Artificial Earth Satellites, (Translated from Russian)," tech. rep., 1967.

[9] I. V. d. Costa and A. F. B. d. Almeida Prado, "Orbital evolution of a satellite perturbed by a third-body," *Adv. Space Dyn*, 2000, pp. 176–194.

[10] M. Lidov, "The evolution of orbits of artificial satellites of planets under the action of gravitational perturbations of external bodies," *Planetary and Space Science*, Vol. 9, No. 10, 1962, pp. 719 – 759, https://doi.org/10.1016/0032-0633(62)90129-0.

[11] Y. Kozai, "Secular perturbations of asteroids with high inclination and eccentricity," *The Astronomical Journal*, Vol. 67, Nov. 1962, p. 591, 10.1086/108790.

[12] C. Colombo, "Long-term evolution of highly-elliptical orbits: luni-solar perturbation effects for stability and re-entry," *25th AAS/AIAA Space Flight Mechanics Meeting*, 2015.

[13] A. J. Rosengren, J. Daquin, K. Tsiganis, E. M. Alessi, F. Deleflie, A. Rossi, and G. B. Valsecchi, "Galileo disposal strategy: stability, chaos and predictability," *Monthly Notices of the Royal Astronomical Society*, Vol. 464, No. 4, 2017, pp. 4063–4076, 10.1093/mnras/stw2459.

[14] I. I. Shevchenko, *The Lidov-Kozai effect-applications in exoplanet research and dynamical astronomy*, Vol. 441. Springer, 2016.

[15] I. Gkolias, J. Daquin, F. Gachet, and A. J. Rosengren, "From Order to Chaos in Earth Satellite Orbits," *The Astronomical Journal*, Vol. 152, No. 5, 2016, p. 119.

[16] B. Katz, S. Dong, and R. Malhotra, "Long-Term Cycling of Kozai-Lidov Cycles: Extreme Eccentricities and Inclinations Excited by a Distant Eccentric Perturber," *Phys. Rev. Lett.*, Vol. 107, Oct 2011, p. 181101, 10.1103/PhysRevLett.107.181101.

[17] S. Naoz, W. M. Farr, Y. Lithwick, F. A. Rasio, and J. Teyssandier, "Secular dynamics in hierarchical three-body systems," *Monthly Notices of the Royal Astronomical Society*, Vol. 431, No. 3, 2013, pp. 2155–2171, 10.1093/mnras/stt302.